Clays and Clay Minerals, Vol. 39, No. 2, 113–126, 1991.

WEATHERING OF GRANITIC MUSCOVITE TO KAOLINITE AND HALLOYSITE AND OF PLAGIOCLASE-DERIVED KAOLINITE TO HALLOYSITE

IAN D. M. ROBERTSON[1] AND RICHARD A. EGGLETON

Centre for Australian Regolith Studies, Australian National University, G.P.O. Box 4
Canberra, ACT 2601, Australia

Abstract—Weathered perthite and mixed muscovite-kaolinite from a kaolinitic granite at Trial Hill in east Queensland and kaolinized sericitic alteration from a granite from the Ardlethan Tin Mine of New South Wales were examined by optical, scanning electron (SEM), and transmission electron microscopy (TEM) to determine the alteration process of muscovite to kaolinite and kaolinite to halloysite (7Å). Muscovite was found intimately interleaved with kaolinite in a variety of proportions on a sub-micrometer scale. The contact was generally parallel to the (001) layers of both minerals, and the thickness of the contact layer alternated between 10 and 7 Å over short distances. Where the kaolinite to muscovite contact was at an acute angle to the muscovite layers, a small angle existed between the layering of the two phases, consistent with a topotactic alteration of muscovite to kaolinite. One tetrahedral sheet in the muscovite appeared to have been removed over 50–100 Å, converting a 10-Å layer to a 7-Å layer. The mica near the contact with kaolinite was easily damaged in the electron beam and showed Al loss during analytical transmission electron microscopy; thus, H_3O^+ probably substituted for K^+ in this transitional phase.

An SEM examination of completely weathered plagioclase showed kaolinite plates having attached, parallel, polygonal rods of halloysite (7Å), which had planar sides and a central void, partly fused with the surfaces of the kaolinite crystals. TEM study showed that the kaolinite altered to halloysite, and that, where the kaolinite was partly altered to halloysite, a series of sharp kinks were present in the kaolinite plate in which alteration had occurred. These kinks were interspersed with linear kaolinite relics, 0.1–0.2 μm long, which appear to have provided local rigidity to the clay packet. Apparently, the altered clay first curled into loosely wound spirals, which ranged in cross-section from triangles to irregular octagons, with pentagons and hexagons being most common. The tendency to pentagons and hexagons compares well with a statistical study of the angles, which were most commonly grouped around 120°. As alteration of the kaolinite relics progressed, the linear parts of the spiral lost their rigidity and became circular or oval shaped. The long axis of the halloysite spirals was parallel to the X axis of the kaolinite. Halloysite spirals formed most readily if they had space to curl; if space was not available, the halloysite formed sheaves. Rare, thin layers of muscovite were present projecting through kaolinite into halloysite. Where muscovite relics reached open spaces, the 10-Å structure expanded to 14 Å.

Key Words—Alteration, Halloysite, Kaolinite, Morphology, Muscovite, Smectite, Transmission electron microscopy, Weathering.

INTRODUCTION

Kaolinite and halloysite are common products of granite weathering and hydrothermal alteration. A mineralogical method for distinguishing between these two processes would be useful for mineral exploration and for interpreting geological history. The major body of work on the morphology of these two kaolin-group minerals is that of Keller and Hanson (1975), Hanson *et al.* (1981), and Keller (1982). The relation between the composition and morphology of halloysite was examined by Tazaki (1981) and Tazaki and Fyfe (1987). The mechanism for curling of halloysite was recently reviewed by Bailey (1989).

The literature contains little information about the paragenesis of kaolinite and halloysite in weathering. Banfield (1985) suggested that coalescence of halloysite tubes could form platey kaolinite. Bailey (1989), in summarizing the properties of kaolinite and halloysite, supposed tetrahedral Al to be essential to the formation of halloysite. The spatial and chemical relations between co-existing halloysite and kaolinite are very scantily documented. In the present study, weathered granites at two tin deposits in Australia were examined by scanning electron microscopy (SEM), electron microprobe, and transmission electron microscopy (TEM). The co-existence of kaolinite and halloysite in these rocks provided an opportunity to examine the paragenetic relationship between the two clay minerals and to assess evidence for chemical and/or temporal relationships.

SAMPLE LOCATION AND EXPERIMENTAL METHODS

Most of the material came from a deeply weathered granite at the Trial Hill Tin Mine in east Queensland.

[1] Present address: Division of Exploration Geoscience, CSIRO, Private Bag, P.O. Wembley, Western Australia 6014, Australia.

The granite has weathered below a pre-Pliocene lateritic surface, which was later uplifted. A small valley was cut into this surface and was subsequently filled with debris-flow sediments and tin-bearing gravels (Robertson, 1990). The whole was later capped by the Pliocene-Pleistocene Nulla Basalt. Additional specimens of intimately mixed muscovite and kaolinite were collected from the middle benches of the Ardlethan Tin Mine of New South Wales in a zone of unusually deep weathering (40 m).

Textural relations were investigated optically, and microprobe analyses, using both a Technische Physische Dienst energy-dispersive and a Cameca wavelength-dispersive electron microprobe, were made on polished thin sections prepared in kerosene. Small specimens of various textural types were removed from the section and studied by X-ray powder diffraction using a Debye-Scherrer camera. The morphology of the clay was examined on a Cambridge scanning electron microscope, equipped with an energy-dispersive X-ray analytical system.

For TEM, Ar-ion-beam-milled specimens, mounted on copper grids and coated with carbon, were viewed on the JEOL 100 CX and 200 CX electron microscopes, using accelerating voltages of 100 and 200 kV respectively, in the Research School of Chemistry at the Australian National University. Analytical electron microscopy (AEM) was carried out on a Philips 430 AEM at the Research School of Earth Sciences, using a cold stage and an accelerating voltage of 300 kV. Specimen heating was kept to a minimum by analyzing as large an area as possible and by using beam astigmation (about 500 × 1500 Å) on elongated phases.

The clay minerals were identified by TEM and AEM using the following criteria: (1) Muscovite, kaolinite, and halloysite have approximately equal Al:Si atomic ratios, muscovite also contains potassium. (2) Muscovite shows 10-Å fringes and/or a 10-Å electron diffraction pattern viewed parallel to (001). (3) Kaolinite shows straight 7-Å fringes and a 7-Å electron diffraction pattern if viewed parallel to (001). (4) Halloysite (7Å) shows a spiral or tubular structure, a 7-Å ring electron diffraction pattern, and no diffraction fringes. No halloysite (10Å) was identified.

Both kaolinite and muscovite exhibited mottled diffraction contrast. Mottled diffraction contrast is the electron microscopic analogue of the "watered-silk" optical birefringence so common in phyllosilicates, although it has a slightly different origin. It is due to a variation in contrast from a slightly wavy phyllosilicate oriented approximately parallel to (001), in which adjacent regions deviate slightly from the ideal Bragg orientation. This mottled diffraction-contrast effect is shown by both kaolinite and muscovite, but not by halloysite, which is not sufficiently ordered crystallographically (either inherently or after electron beam exposure) to develop mottled diffraction contrast. Both kaolinite and halloysite damaged rapidly in the electron beam, halloysite damaging the more readily. Halloysite spirals, however, did not change significantly in either shape or curvature during electron beam exposure until catastrophic damage occurred.

RESULTS

Optical microscopy

Weathered granite from the Trial Hill Tin Mine. Specimens of mixed muscovite, kaolinite, and halloysite were selected for TEM study from a white, highly kaolinized granite. The kaolinite was, in part, stained yellow-brown by iron oxides. It also contained a very small amount of illite. Large, composite grains of angular and in part sutured, strained quartz, 0.4–4.0 mm in size, and irregular remnants of potassium feldspar were noted in a complex kaolinitic groundmass. Quartz was the only completely unaltered mineral. Anhedral, brown, clouded potassium feldspar showed Carlsbad twinning, cleavage, and a perthitic structure. It had a rather undulose extinction and consisted of domains separated by kaolinite. Only the potassium feldspar component ($Ab_{3-5}An_0Or_{95-97}$) of the original perthite remained. The plagioclase component of the perthite had been completely converted to extremely fine grained, very low birefringent clay (Figure 1A)

In contrast, plagioclase crystals of the granite, which were recognized by their gross morphology, had been completely weathered and pseudomorphed by fine- and coarse-grained kaolinite (Figure 1B). The fine-grained kaolinite (0.005–0.1 mm) formed patches 0.5–4.0 mm in size, having a matted fabric and grey birefringence. It coexisted with distorted stacks, books, and mats of a coarser-grained mixture of kaolinite and muscovite (0.05–1.0 mm). The kaolinite-muscovite mixture was also of two types: one was a texturally uniform material (Figure 1C), having a birefringence which ranged gradationally from dark-grey to first-order yellow. The other consisted of thin, but optically discrete layers of extremely low birefringent clay, interleaved with platey, highly birefringent (second-order blue-green) muscovite. The contact between these two minerals was sharp. Locally, the clay formed wedges between muscovite cleavage plates (Figure 1D).

Weathered granite from the Ardlethan tin mine. The rock was pale-grey and had a granitic fabric. In thin section, this specimen consisted of shards of coarse-grained, strained, sutured quartz, set in a groundmass of sericite and smaller quartz fragments. Patches and bent flakes of muscovite and chlorite were present in the matrix, coexisting with and interleaved with opaque minerals. Patches of very fine grained sericite and some kaolinite were present as fragments and contained flakes of muscovite. The matrix consisted of coarser-grained kaolinite, sericite, and opaque minerals.

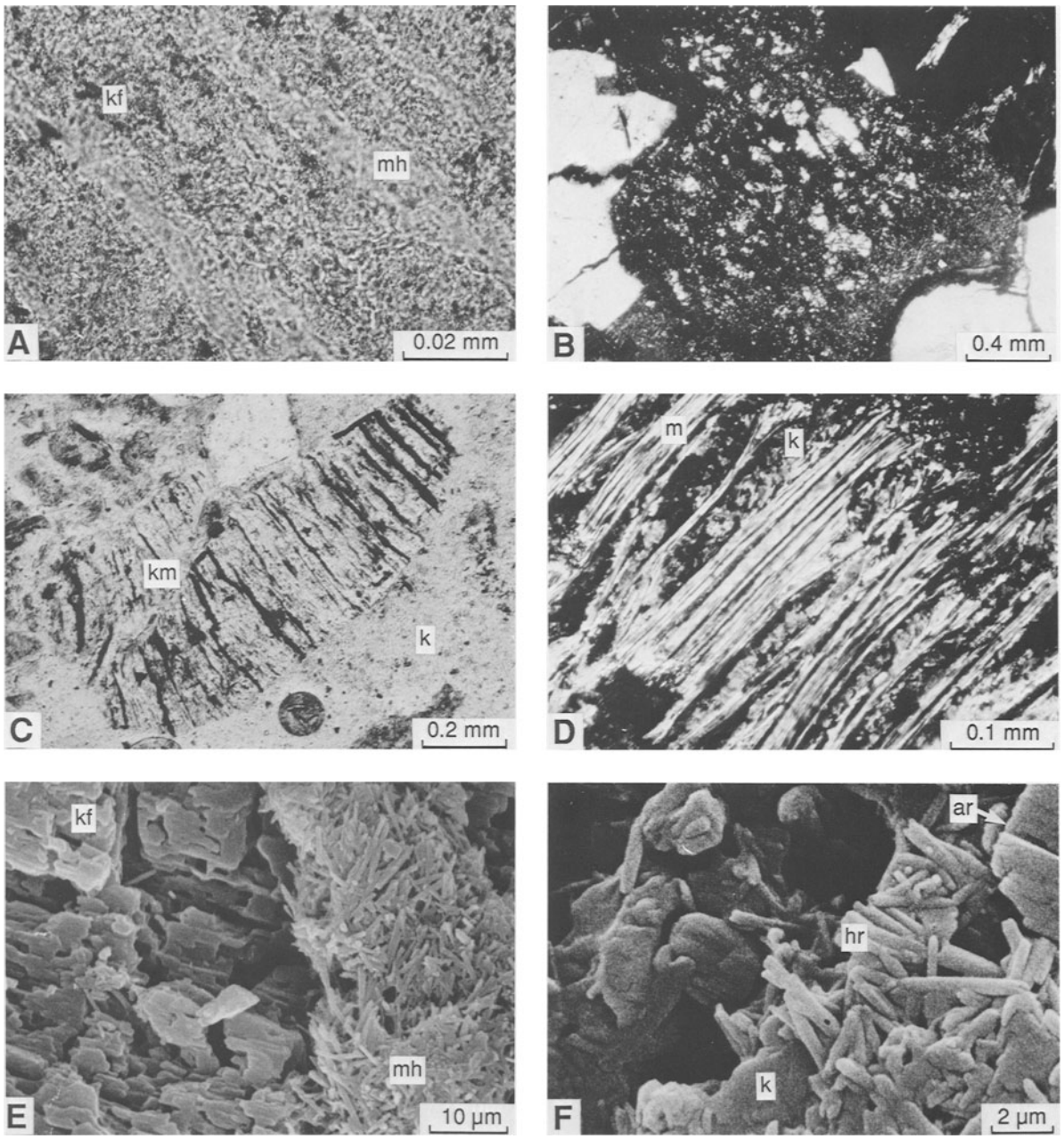

Figure 1. Optical micrographs of kaolinite and mica in weathered granite, Trial Hill Mine: (A) very fine grained halloysite (mh) that has completely replaced plagioclase in vein perthite (kf) (plane polarized light); (B) plagioclase crystal replaced by kaolinite and flecked with coarse-grained kaolinite and muscovite (crossed polarizers); (C) elongated book of intimately mixed but optically uniform kaolinite and muscovite (km) set in fine-grained kaolinite (k) (plane polarized light); (D) book of muscovite (m) wedged apart by very fine grained kaolinite (k) (crossed polarizers). Scanning electron micrographs of feldspar pseudomorphs, weathered granite, Trial Hill Mine: (E) partly pseudomorphed vein perthite; mesh of halloysite rods (mh), after plagioclase of vein perthite, surrounded by an etched microcline lacework (kf); (F) plagioclase pseudomorph; halloysite rods, some with planar sides (hr) and kaolinite plates (k), some with attached halloysite rods (ar).

Microprobe analyses

Microprobe analysis of the different kaolinite phases from the Trial Hill weathered granite showed a variety of compositions. The kaolinized component of the perthite and the kaolinized plagioclase had the average structural formulae given in Table 1. In each, the Si/Al atomic ratios were greater than unity, the expected value for pure kaolinite (average 1.08). Microprobe analyses of the mixed kaolinite-mica, which occurred

https://doi.org/10.1346/CCMN.1991.0390201 Published online by Cambridge University Press

Table 1. Average elemental ratios of kaolinites derived from two contrasting plagioclase types (based on 14 oxygens).

	Original mineral		
	Perthite plagioclase	Separate plagioclase	
Si	4.13	4.24	3.99
Al	3.71	3.44	3.88
Ti	0.00	0.01	0.00
Fe^{3+}	0.06	0.11	0.06
Mn	0.00	0.00	0.00
Mg	0.04	0.10	0.06
Ca	0.02	0.04	0.03
Na	0.01	0.01	0.00
K	0.04	0.08	0.02
Number of analyses	6	2	9

as inclusions in the pseudomorphs of the separate plagioclase phase (Table 2), showed that the weakly birefringent type ranged widely in both K_2O (0.22–5.85%) and Fe_2O_3 (0.43–6.23%). The birefringence seemed related to iron but not to potassium. Analyses of kaolinite interleaved with muscovite are given in Table 3. The Si/Al atomic ratios are also all greater than unity (average 1.19).

The muscovite of the weathered granite (Table 4, specimens MJ6 and MJ9) may be compared with muscovites of the underlying fresh granite (specimen MJ10). The Si/Al ratio ranged from 1.29 in fresh muscovite to 1.07 in muscovite from weathered granite, and a range of Fe, Mg, and K contents is apparent for the weathered material.

Scanning electron microscopy

The overall fabric of the altered perthite is shown in Figure 1E. The potassium feldspar is deeply etched and has a delicate lace-like structure. A mesh of randomly oriented halloysite rods, 3 μm in length, was noted pseudomorphic after the plagioclase of the perthite and in veinlets in the etched feldspar. The kaolinized pseudomorphs after plagioclase show an open mesh of plates of kaolinite (2–3 μm in size, identified by qualitative microprobe analysis, morphology, and XRD data) set with randomly oriented rods of halloysite (1–3 μm long × 0.1 μm wide). Stereo-imaging of the halloysite rods revealed that they had polygonal, not circular, cross-sections and flat faces parallel to their long axes. Some had a central void. Many halloysite rods lay on the kaolinite plates, and the two appeared to be attached (Figure 1F). Examination of further detail was limited by the resolution of the SEM

Transmission electron microscopy

The various clays derived from different feldspar phases at the Trial Hill Tin Mine and the mixed kaolinite-muscovite material from the Ardlethan Tin Mine were each examined by TEM. The clay mineral

Table 2. Mixed kaolinite-micas of specimen MJ7 and MJ11, Trial Hill.

	Analysis number											
	7.26	7.27	7.28	7.29	7.30	7.31	7.32	7.34	7.35	7.36	7.37	Mean
SiO_2	44.31	45.70	46.37	43.31	43.68	37.77	45.55	48.19	43.86	50.83	49.50	45.37
TiO_2	0.00	0.00	0.00	0.00	0.00	0.00	0.00	0.00	0.00	0.00	0.04	0.00
Al_2O_3	36.56	37.04	37.47	35.93	35.91	30.68	39.93	38.54	30.72	39.62	39.32	36.52
Fe_2O_3	0.98	1.12	0.96	0.78	0.79	1.80	0.64	0.96	3.60	1.00	1.07	1.24
MnO	0.00	0.11	0.04	0.00	0.00	0.05	0.00	0.00	0.00	0.04	0.00	0.02
MgO	0.23	0.19	0.15	0.16	0.13	0.33	0.08	0.09	0.71	0.17	0.18	0.22
CaO	0.10	0.13	0.07	0.09	0.05	0.12	0.04	0.05	0.36	0.10	0.03	0.10
Na_2O	0.03	0.07	0.03	0.06	0.23	0.08	0.00	0.16	0.02	0.00	0.03	0.06
K_2O	1.66	3.03	2.25	1.13	2.99	1.36	0.22	4.13	0.27	1.20	2.45	1.88
	83.87	87.39	87.34	81.46	83.78	72.19	86.46	92.12	79.54	92.96	92.62	85.42
	Elemental ratios based on 14 oxygens											
Si	3.979	3.982	4.011	3.986	3.968	3.963	3.919	4.002	4.157	4.090	4.037	4.010
Al	3.870	3.804	3.820	3.897	3.845	3.794	4.049	3.772	3.431	3.757	3.779	3.804
Ti	0.000	0.000	0.000	0.000	0.000	0.000	0.000	0.000	0.000	0.000	0.002	0.000
Fe^{3+}	0.066	0.074	0.062	0.054	0.054	0.142	0.042	0.060	0.257	0.061	0.065	0.083
Mn	0.000	0.008	0.003	0.000	0.000	0.004	0.000	0.000	0.000	0.003	0.000	0.001
Mg	0.031	0.025	0.019	0.022	0.018	0.052	0.010	0.011	0.101	0.020	0.022	0.029
Sum	3.966	3.910	3.904	3.973	3.916	3.992	4.101	3.843	3.788	3.841	3.869	3.917
Large cations												
Ca	0.010	0.012	0.006	0.009	0.005	0.013	0.004	0.004	0.037	0.009	0.003	0.009
Na	0.005	0.012	0.005	0.011	0.041	0.016	0.000	0.026	0.004	0.000	0.005	0.011
K	0.190	0.388	0.248	0.133	0.347	0.182	0.024	0.438	0.033	0.123	0.255	0.212
Sum of large cations	0.205	0.361	0.260	0.152	0.392	0.212	0.028	0.468	0.073	0.132	0.262	0.232

https://doi.org/10.1346/CCMN.1991.0390201 Published online by Cambridge University Press

assemblage derived from each parent is described separately below.

Perthite—Trial Hill. The potassium feldspar, identified by its electron diffraction pattern, was unaltered. It showed a smooth, slightly curved edge against the completely altered plagioclase perthite component, now clay (Figure 2A). This clay component consisted entirely of randomly oriented, rolled tubes of halloysite of 0.08–0.15 μm cross section and 0.5 μm length. Most showed polygonal cross sections (Figures 2A–2D), though a few were oval (Figures 2B and 2C) or in part oval (Figure 2C). All showed hollow centers (Figures 2A–2D), and many showed wedge-shaped voids near the angles of the polygons (Figure 2A). Longitudinal sections generally showed a central void (Figures 2B and 2D). The halloysite was very readily damaged by the electron beam (Figures 2C and 2D). Although the halloysite was recognized on morphological grounds, its slightly granular ring diffraction pattern showed typical reflections at 7.2, 4.4, 3.6, and 2.6 Å.

Although some halloysite rods had tube-like cross sections, many had cross-sections represented by irregular polygons ranging from triangles to octagons. Both the frequency of occurrence of these shapes and the angles subtended by the polygons were examined statistically from a large number of electron micrographs and are compared in Figure 3. The most common angles group around 120°. The occurrence of the most common angles is strongly correlated with the occurrence of the most common shapes, i.e., pentagons and hexagons.

No platey kaolinite was seen in the weathered perthite, although some parts of halloysite longitudinal and cross sections showed patches of mottled diffraction contrast where the halloysite section was particularly straight and where the cross-sections were invariably polygonal, rather than tubular (Figure 2A).

Kaolinized plagioclase—Trial Hill. Electron diffraction patterns of weathered plagioclase from Trial Hill show either oriented kaolinite and randomly oriented halloysite or interleaved muscovite and kaolinite. Diffraction patterns of the mixed kaolinite-muscovite showed that kaolinite was slightly fanned, whereas muscovite was not. Strong streaking in the $k = 2$ row on $0kl$ electron diffraction patterns indicated stacking disorder in one of the materials, presumably the kaolinite.

The kaolinite and muscovite phases were interleaved as discrete packets (Figures 7 and 10B). Narrow, dark strips of muscovite, showing mottled diffraction contrast, lay within and parallel to layers of kaolinite. Some of the kaolinite occurred in vermiform stacks, with partings at 0.05–0.15-μm intervals. Halloysite rods were present in voids between the kaolinite books and stacks.

Table 2. Continued.

Analysis number												
11.39	11.40	11.41	11.42	11.43	11.44	11.45	11.47	11.48	11.49	11.50	11.51	Mean
39.29	37.27	46.33	31.11	40.20	38.89	29.71	26.23	49.22	54.27	45.68	45.15	40.28
0.00	0.00	0.00	0.03	0.00	0.00	0.00	2.33	0.07	0.05	0.00	0.07	0.21
31.02	30.34	35.92	25.40	33.31	28.50	25.01	18.36	32.60	33.40	27.95	30.63	29.37
1.29	0.99	0.43	1.22	0.74	1.88	0.58	1.99	4.87	6.05	6.23	4.28	2.54
0.00	0.00	0.05	0.05	0.07	0.00	0.00	0.15	0.05	0.00	0.06	0.00	0.04
0.20	0.14	0.00	0.14	0.00	0.28	0.11	0.61	0.42	0.66	0.59	0.52	0.31
0.12	0.10	0.00	0.11	0.02	0.18	0.04	0.02	0.31	0.43	0.41	0.39	0.18
0.02	0.20	0.17	0.10	0.18	0.08	0.19	0.13	0.00	0.00	0.02	0.00	0.09
1.44	3.47	5.11	2.35	5.85	2.73	3.70	5.83	0.23	0.40	0.43	0.28	2.65
73.38 high	72.51 mod	88.01 low	60.51	80.37	72.54 low	59.34	55.65 mod	87.77 high	95.26 high	81.37 high	81.32 high	75.67
Elemental ratios based on 14 oxygens												
4.037	3.952	4.051	3.941	3.905	4.103	3.886	3.842	4.232	4.312	4.279	4.193	4.082
3.757	3.792	3.702	3.792	3.814	3.543	3.855	3.170	3.304	3.128	3.085	3.352	3.508
0.000	0.000	0.000	0.003	0.000	0.000	0.000	0.257	0.005	0.003	0.000	0.005	0.016
0.100	0.079	0.029	0.117	0.054	0.149	0.057	0.219	0.315	0.362	0.439	0.299	0.104
0.000	0.000	0.004	0.005	0.006	0.000	0.000	0.019	0.004	0.000	0.005	0.000	0.003
0.031	0.022	0.000	0.026	0.000	0.044	0.021	0.133	0.054	0.078	0.082	0.072	0.047
3.887	3.893	3.734	3.943	3.874	3.736	3.934	3.798	3.681	3.571	3.612	3.728	3.786
0.013	0.011	0.000	0.015	0.002	0.020	0.006	0.003	0.029	0.037	0.041	0.039	0.020
0.004	0.041	0.029	0.025	0.034	0.016	0.048	0.037	0.000	0.000	0.004	0.000	0.018
0.189	0.469	0.570	0.380	0.725	0.367	0.617	1.090	0.025	0.041	0.051	0.033	0.343
0.206	0.522	0.599	0.419	0.761	0.404	0.671	1.130	0.054	0.077	0.096	0.072	0.380

https://doi.org/10.1346/CCMN.1991.0390201 Published online by Cambridge University Press

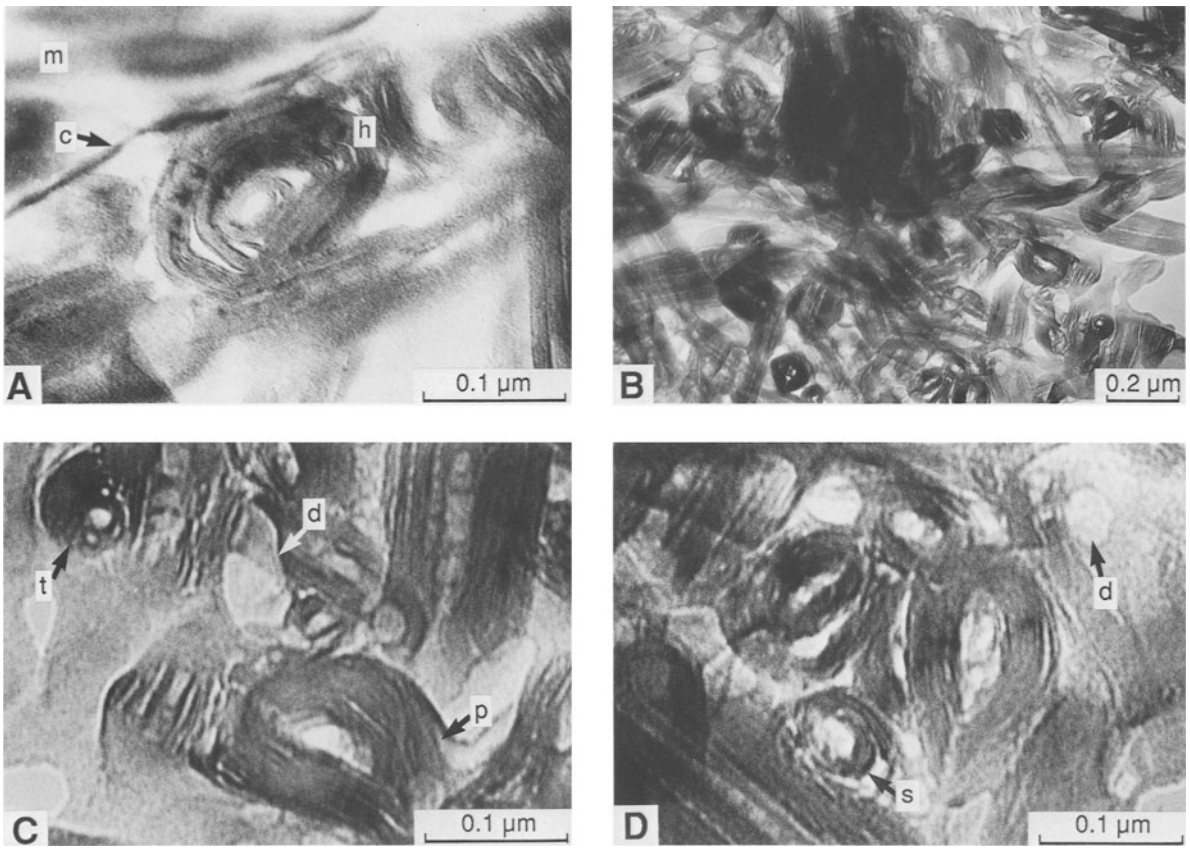

Figure 2. Transmission electron micrographs of halloysite sections: (A) spiral polygonal halloysite cross section (h) abutting unaltered microcline (m) along a smooth contact (c); note mottled diffraction contrast in linear parts of halloysite polygon and triangular voids at angles in polygon; (B) variety of cross sections, ranging from tubular to polygonal and some longitudinal sections, all showing central voids; (C) large, partly polygonal and partly oval cross section (p) and a smaller tubular halloysite cross section (t) enlarged from (B); note electron beam damage (d); (D) several partly oval, partly polygonal tubular and spiral cross sections; note primitive spiral (s) and electron beam damage (d).

Figure 4 shows strips of kaolinite that are continuous with loosely wound spirals of halloysite. A series of sharp kinks exist along the kaolinite crystal at 0.1–0.2-μm intervals, in which the clay structure is rather indistinct (halloysite). These kinks are interspersed with linear relics of kaolinite, showing mottled diffraction contrast (Figure 5 (upper)). The most common forms of the halloysite spirals are irregular pentagons and hexagons; less-common are quadrilaterals and triangles. Wedge-shaped gaps in the halloysite occur at or near the kink points, the whole resembling a rolled newspaper. In places the halloysite rods have smoothly curved, oval, or circular cross-sections.

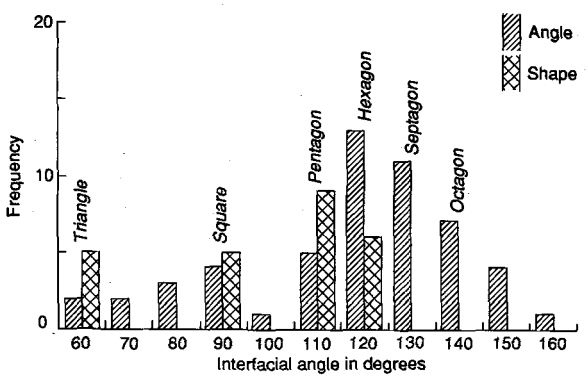

Figure 3. Correlation between frequency distribution of interfacial angles and shapes of halloysite polygons.

The TEM morphology supports in detail the SEM observations (above) of polygonal halloysite rods having a central void, and kaolinite platelets having polygonal halloysite rods attached to their surfaces (shown diagramatically in Figure 5 (lower)).

Low birefringent mixed kaolinite-mica booklets—Trial Hill. Kaolinite-mica booklets were noted containing rolled tubes of halloysite and showing slightly fanned kaolinite layers. Only a few muscovite diffraction patterns were obtained, although some images of the sheet-like kaolinite show small wisps of remnant muscovite (10-Å fringes). Flakes of kaolinite at the edge of a void or in a split in the kaolinite packet were detached from

https://doi.org/10.1346/CCMN.1991.0390201 Published online by Cambridge University Press

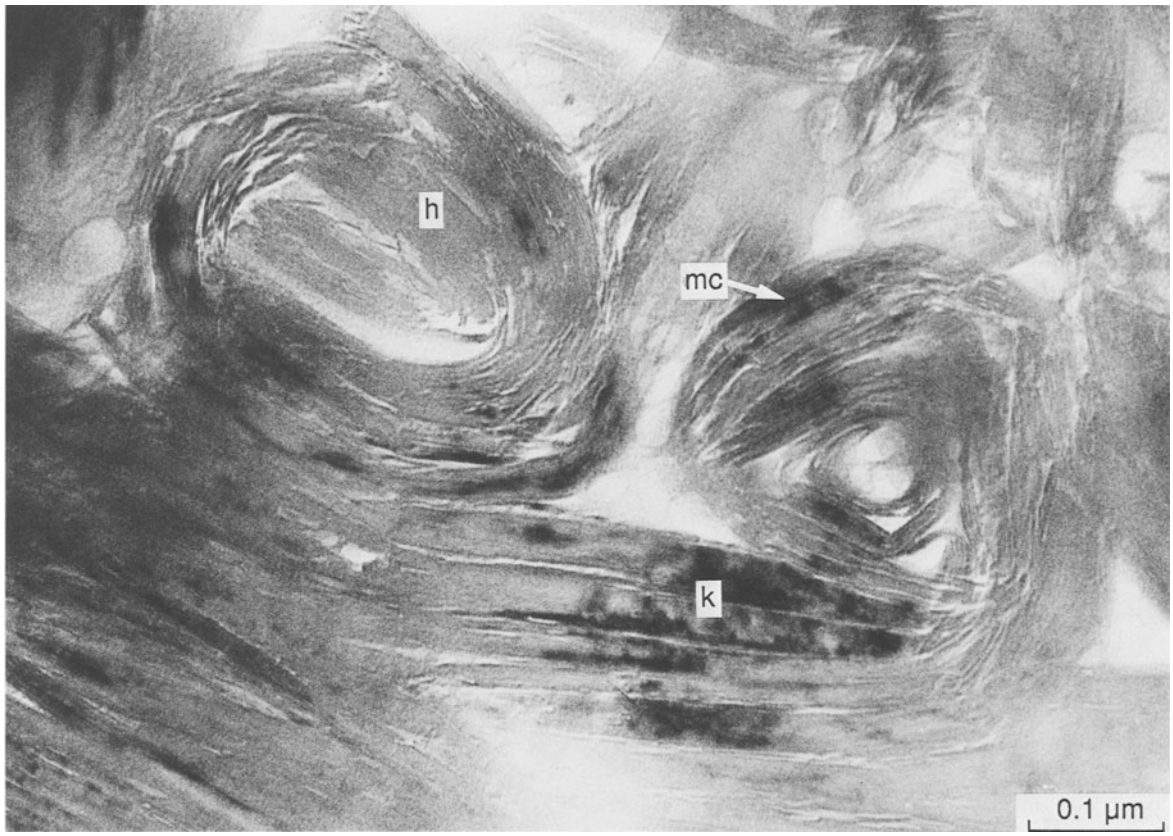

Figure 4. Transmission electron micrographs of strips of kaolinite (k) continuous with polygonal and oval rolls of halloysite (h). Parts of the halloysite spirals contain straight sections, similar to kaolinite (mottled diffraction contrast, mc).

Table 3. Compositions of kaolinite interleaved in muscovite in specimen MJ9, Trial Hill.

	Analysis number						
	9.25	9.26	9.27	9.28	9.29	Mean	s.d.
SiO_2	48.73	47.33	48.36	48.69	48.50	48.32	0.57
TiO_2	0.00	0.02	0.03	0.04	0.03	0.02	0.02
Al_2O_3	34.78	33.93	35.29	33.62	34.63	34.45	0.67
Fe_2O_3	3.10	3.01	3.32	3.47	3.32	3.24	0.21
MnO	0.00	0.00	0.00	0.00	0.00	0.00	0.00
MgO	0.36	0.33	0.30	0.48	0.37	0.37	0.07
CaO	0.31	0.25	0.28	0.42	0.35	0.32	0.07
Na_2O	0.04	0.04	0.05	0.03	0.04	0.04	0.01
K_2O	0.43	0.65	0.36	0.33	0.33	0.42	0.13
	87.75	85.56	87.99	87.08	87.57	86.18	–
	Elemental ratios based on 14 oxygens						
Si	4.169	4.160	4.130	4.203	4.161	4.165	0.026
Al	3.507	3.515	3.552	3.420	3.501	3.499	0.048
Ti	0.000	0.001	0.002	0.003	0.002	0.001	0.001
Fe^{3+}	0.200	0.199	0.213	0.225	0.214	0.210	0.011
Mn	0.000	0.000	0.000	0.000	0.000	0.000	0.000
Mg	0.046	0.043	0.038	0.062	0.047	0.048	0.009
Sum	3.753	3.758	3.806	3.710	3.765	3.759	0.034
Large cations							
Ca	0.028	0.024	0.026	0.039	0.032	0.030	0.006
Na	0.007	0.007	0.008	0.005	0.007	0.007	0.001
K	0.047	0.073	0.039	0.036	0.036	0.046	0.015
Sum of large cations	0.082	0.103	0.073	0.081	0.075	0.082	0.012

https://doi.org/10.1346/CCMN.1991.0390201 Published online by Cambridge University Press

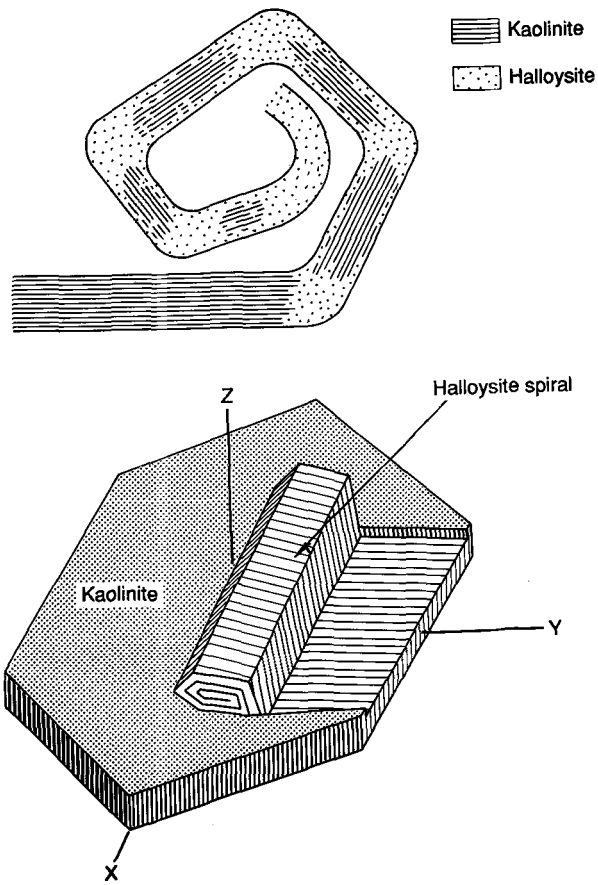

Figure 5. (Upper) Model for halloysite spiral development. Hydration of kaolinite to halloysite has occurred at points along a kaolinite crystal. At these points halloysite curls. Intervening kaolinite relics provide localized rigidity, so a polygonal spiral develops. As these relics are progressively consumed, the halloysite curls smoothly. (Lower) Halloysite spiral developed on and attached to a kaolinite plate, by rolling up part of the plate. Compare with (ar) in Figure 1F.

the main body of kaolinite (Figure 6A) and are curled into rolled, irregular, polygonal halloysite rods (Figures 6B and 6C). Here, simple spiral halloysite structures were particularly evident.

If the diffraction patterns indicated kaolinite and very minor muscovite, the corresponding images were principally of kaolinite (which rarely showed fringes because of beam damage). This kaolinite lay parallel to and included muscovite, which makes up at most a third of the whole—generally much less. Both kaolinite and muscovite show mottled diffraction contrast. Some images show muscovite layers grading to kaolinite layers along (001) (or *vice versa*) (Figure 7). The kaolinite patches of low to moderate birefringence contain less included muscovite, compared with kaolinite having a higher birefringence.

Halloysite is relatively rare in this material and occurs either at the ends of the phyllosilicate books, in

Table 4. Average muscovite elemental ratio based on 11 oxygens in weathered and fresh granite, Trial Hill.

Specimen	Weathered granite MJ6	Weathered granite MJ9	Fresh granite MJ10
Si	3.142	3.210	3.222
Al^{IV}	0.858	0.790	0.778
Al^{VI}	2.082	1.713	1.720
Ti	0.000	0.005	0.005
Fe^{2+}	0.080	0.288	0.231
Mn	0.000	0.013	0.010
Mg	0.018	0.085	0.116
Ca	0.003	0.000	0.002
Na	0.013	0.025	0.032
K	0.396	0.837	0.849
Number of analyses	3	2	10

which the kaolinite structure is frayed and wispy, or (Figure 6D) in partings in the phyllosilicate.

Intergrown kaolinite and highly birefringent muscovite—Trial Hill. The electron diffraction patterns of intergrown kaolinite and highly birefringent muscovite indicate kaolinite, muscovite, and halloysite. The muscovite $k = 2$ layer reveals a 20-Å (2-layer) spacing and some very slight streaking in both the $k = 2$ and the [001] rows, indicating the $2M_1$ polymorph, with minor stacking disorder and possibly variation in basal spacing.

The images show two separate morphologies—platey and tubular. The platey phyllosilicate consisted of muscovite, showing mottled diffraction contrast and 10-Å fringes, some of which pass into 7-Å kaolinite fringes. Because of damage to the kaolinite, only a few images were obtained that showed the fringes of the two phases in contact. The contact invariably closely paralleled (001) of both minerals, with the fringes changing spacing in a stepwise manner. Although, in general, the dominant muscovite occupied large zones, locally the muscovite and kaolinite were intimately mixed. Long strips of relict muscovite, which here comprised <5% of the whole, showed 10-Å fringes, which deeply penetrated the kaolinite. In many locations, the muscovite was only two or three fringes wide, but continued for a considerable distance. Fringes along the contact pinched and swelled along their length, one 10-Å layer of muscovite locally collapsed to a 7-Å kaolinite structure and then returned to 10-Å layer further along. Lensoid voids, 0.01 μm wide and 0.1 μm long, separated the structure at 0.05-μm intervals in an *en echelon* pattern. In other parts, slightly fanned, sheet-like kaolinite occurred alone, showing mottled diffraction contrast.

Halloysite was most common at the ends of books of kaolinite, near voids. Here, the mottled diffraction contrast of the kaolinite crystal ended abruptly, and the packet became curved and sheaf-like (Figure 6E),

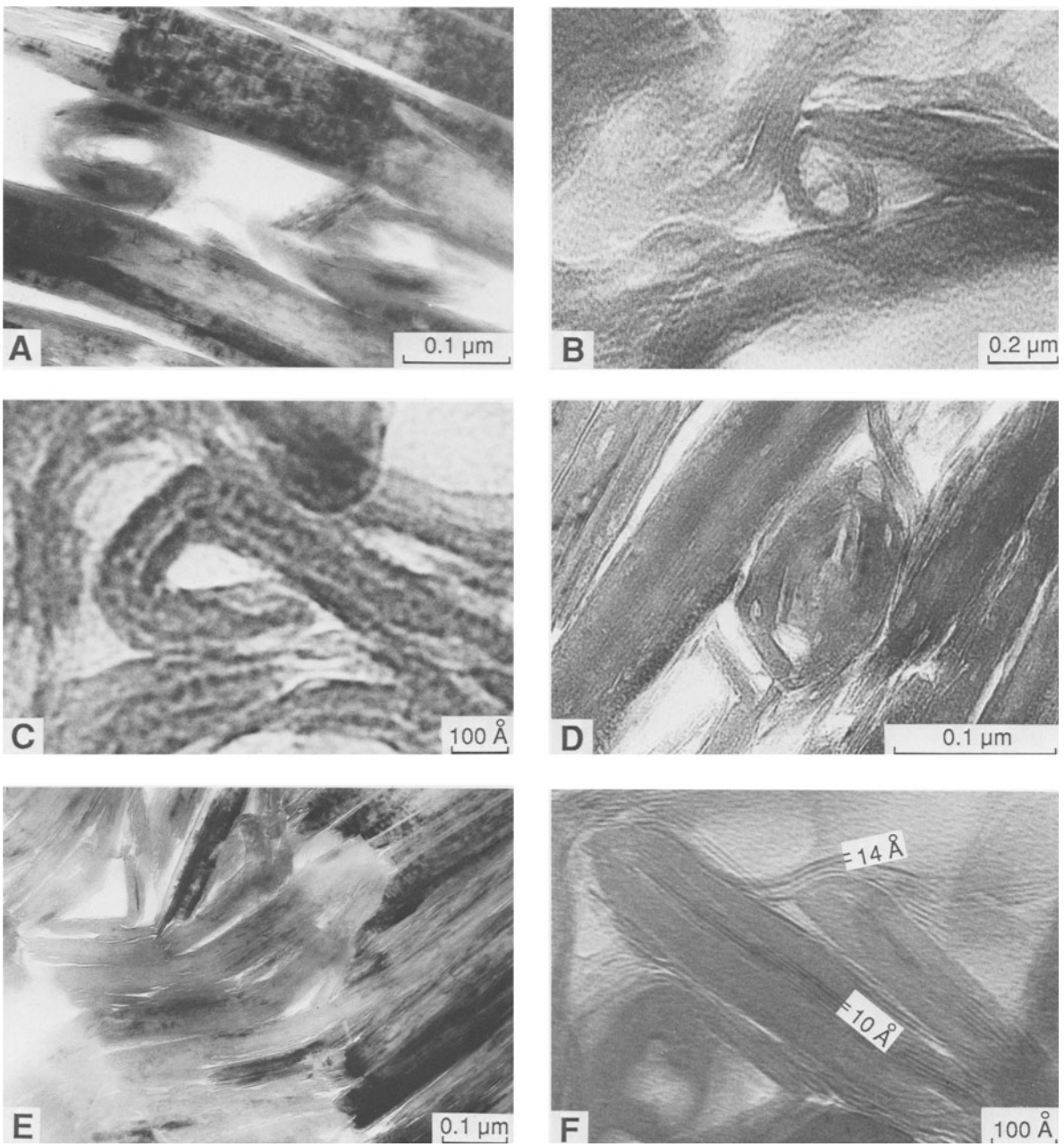

Figure 6. Transmission electron micrographs of halloysite structures in weakly birefringent mixed kaolinite and muscovite booklets: (A) small parting in mottled diffraction contrasted kaolinite, containing halloysite spirals; remnant kaolinite (mottled diffraction contrast) occurs in linear parts of halloysite spirals; (B and C) small, simple halloysite polygonal spirals showing about 410° and 220° of spiral rotation respectively; in B the halloysite spiral is attached to straight kaolinite; (D) tight halloysite spiral in parting in kaolinite; (E) kaolinite (dark, mottled diffraction contrast) largely altered to halloysite (lacking mottled diffraction contrast), which, in turn, has bent and formed sheaves where space was available; (F) halloysite tube containing relics of muscovite (10-Å structure) and attached wisps of a 14-Å structure in the void between halloysite tubes.

interpreted as the transition to halloysite. Elsewhere, some 10-Å layers, only a few fringes in width, extended from the kaolinite structure into the halloysite sheaf (Figure 6F). A few whiskers of a 14-Å structure were noted between the halloysite rolls and sheaves.

Tubular halloysite was relatively scarce. In places the kaolinite structure appeared split, and rolls of halloysite occurred in the voids. The halloysite showed the familiar polygonal cross-sections, ranging in size from 0.05 to 0.35 μm. In Figure 8A, several halloysite

https://doi.org/10.1346/CCMN.1991.0390201 Published online by Cambridge University Press

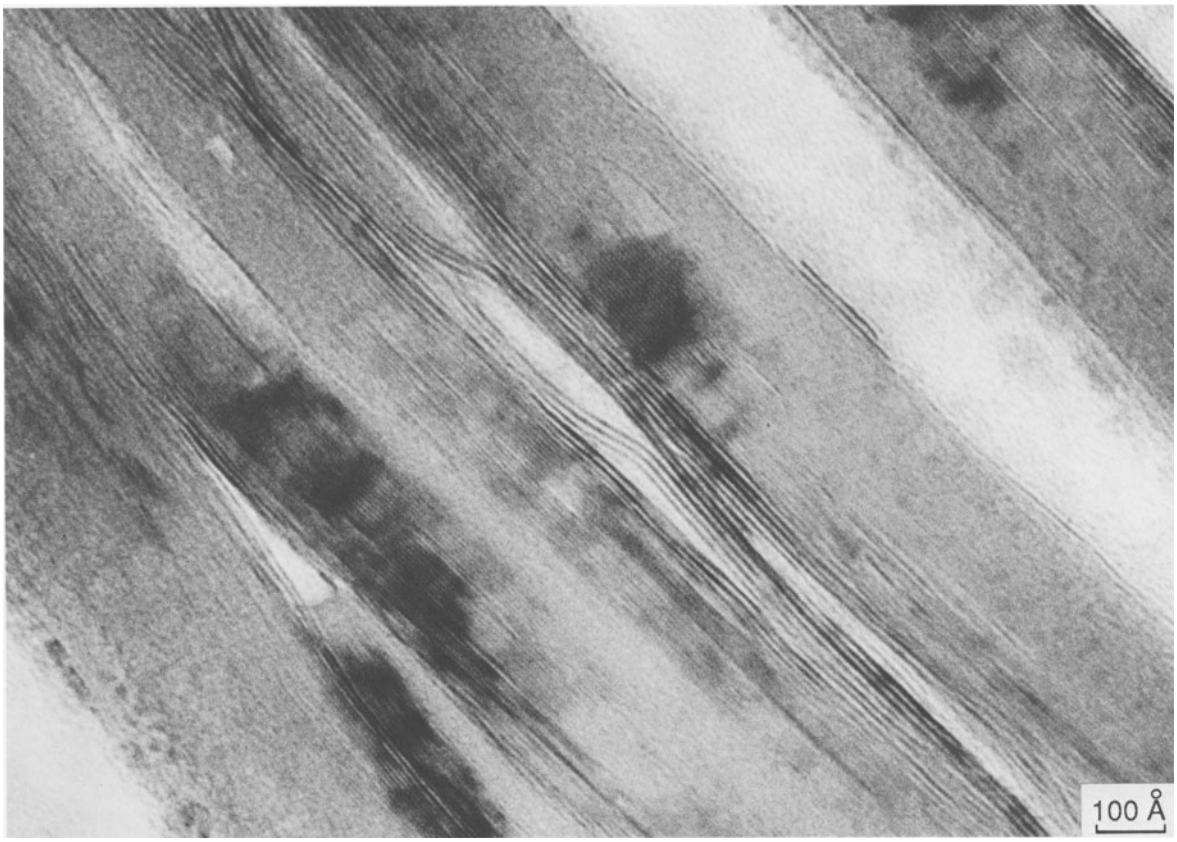

Figure 7. Transmission electron micrograph showing very thin, interleaved, parallel muscovite and kaolinite, both showing mottled diffraction contrast.

rolls, showing well-developed spiral cross sections, can be seen among the kaolinite packets. The diffraction pattern from the layers of kaolinite in contact and continuous with the halloysite (showing 7.1- and 4.4-Å reflections) indicates that the long axis of the halloysite roll was parallel to the X-axis of the kaolinite, shown diagramatically in Figure 8B. The halloysite rolls exhibited triangular, quadrilateral, pentagonal, oval, and circular cross sections.

AEM analyses of areas of unaltered muscovite, platey kaolinite, and their derived tubular halloysite, all showed reasonable compositions, although some were slightly low in Al relative to Si (Table 5, Figures 9A and 9B). Areas of muscovite (identified from 10-Å lattice fringes and mottled diffraction contrast) close to the transition region to kaolinite consistently showed a marked depletion in Al relative to Si (Table 5, reaching an Al:Si atomic ratio as small as 0.2). Successive 20-s analyses of such areas showed a steady drop in the intensity of the Al (Figure 9C) and K characteristic X-ray emission with time, indicating mobilization of these elements in the electron beam. The successive analyses showed little variation in total counts for Si. Such regions only approximated the stoichiometry of mica if they were analyzed immediately after the region was moved into the electron beam. Even taking a photograph was sufficient to remove some Al and K, despite using a beam current less than that used for nanoprobe analysis. This loss of Al during analyses may also explain the slightly low Al content relative to stoichiometry in the kaolinite and halloysite ATEM and microprobe analyses.

Mixed kaolinite and muscovite—Ardlethan Tin Mine. The kaolinite showed a sharp diffraction pattern with some very light streaking in the [00*l*] row, indicating some layer thickness disorder. This layer thickness disorder was confirmed by images that showed numerous splits in the structure and layer terminations. Diffraction patterns of the muscovite showed a 20-Å layer spacing in the k = 2 layer of the 0*kl* plane, with only very slight streaking, suggesting a small amount of stacking disorder and a $2M_1$ muscovite polymorph.

In places, packets of muscovite, 0.1 μm wide, were noted in contact with packets of kaolinite. The contact was sharp, linear and parallel to (001) (Figure 10A) and very rarely cut acutely across the layering. Rippling of both phases and Ar-beam etching along the contact made it difficult to follow each layer. If the phase boundary cut acutely across the layering, there was a

https://doi.org/10.1346/CCMN.1991.0390201 Published online by Cambridge University Press

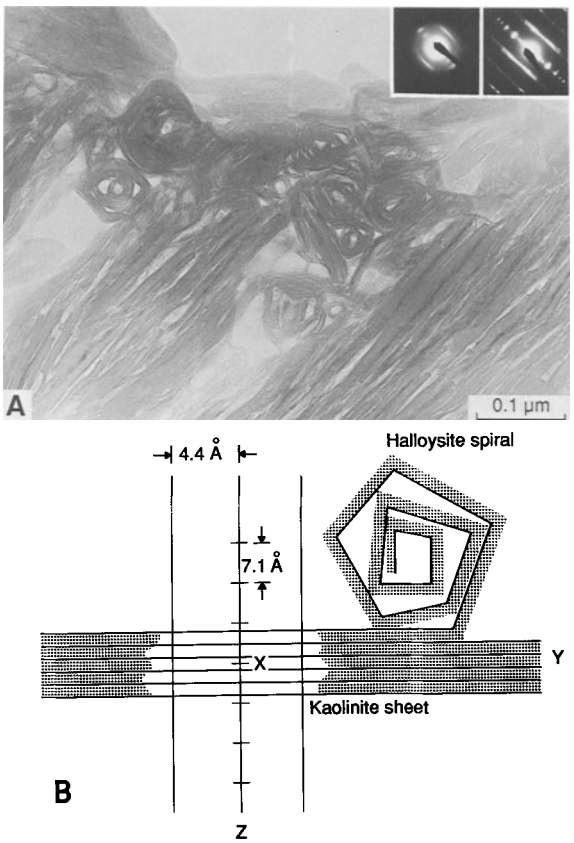

Figure 8. Transmission electron micrographs showing (A) halloysite rolls in contact and continuous with kaolinite layers; axis of halloysite tube is parallel to *X* axis of kaolinite; and (B) crystallographic relationship of the kaolinite plates in A and its attached halloysite roll and the electron diffraction pattern from the kaolinite.

Table 5. Mean elemental ratios from X-ray energy-dispersive analyses (based on 22 oxygens).

	Halloysite	Kaolinite	Muscovite	Transition phase
Si	4.000	4.000	6.000	6.000
Al	3.220	3.765	5.200	1.536
K	0.029	0.024	0.960	0.046
Ca	0.029	0.015	0.000	0.009
Ti	0.002	0.004	0.000	0.004
Fe	0.074	0.126	0.260	0.060

very small angle between the layering of the two phases (Figure 10B). Parts of the image were only just sufficiently sharp to show triple 3-Å structure image layers in the muscovite and double layers in the kaolinite, although slight changes in orientation make interpretation of the contact zone difficult. The change in layer spacing from one mineral to the other took place over 50–100 Å along (001). One of the mica 3-Å fringes became weak and eventually faded out at the contact, suggesting that one layer of muscovite transformed to

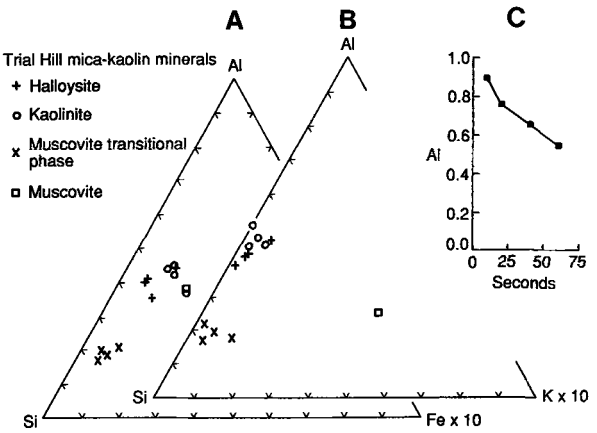

Figure 9. (A and B) Ternary diagrams of semiquantitative analyses of halloysite, kaolinite, and muscovite phases by analytical electron microscopy. Kaolinite and halloysite compositions are indistinguishable. (C) Loss of Al in a muscovite transitional phase during repeated analysis of the same spot.

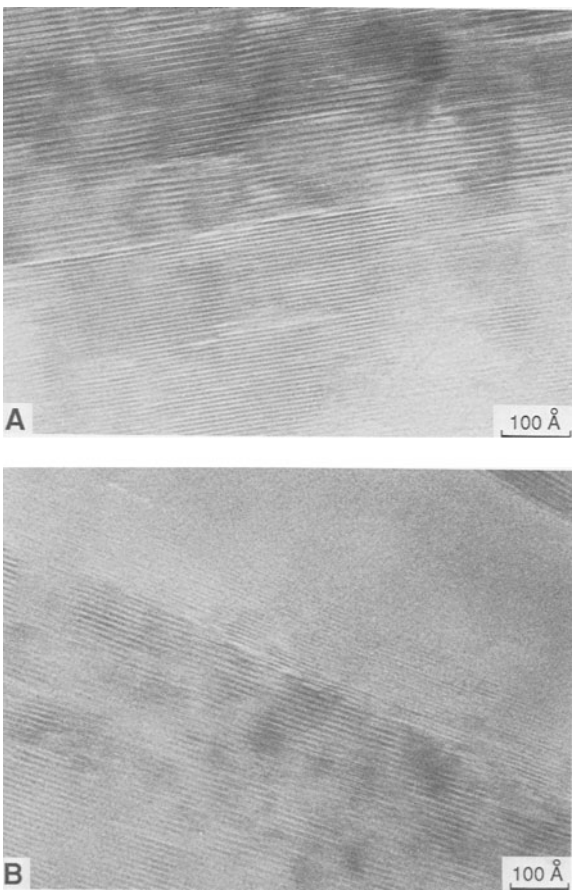

Figure 10. Transmission electron micrographs showing: (A) detail of boundary between kaolinite and muscovite; single fringes alternate from 10 to 7 Å along this contact; both phases show mottled diffraction contrast; (B) muscovite and kaolinite in oblique contact; boundary between kaolinite and muscovite lies at an acute angle to the muscovite layering, and fringes in each phase are not quite parallel.

https://doi.org/10.1346/CCMN.1991.0390201 Published online by Cambridge University Press

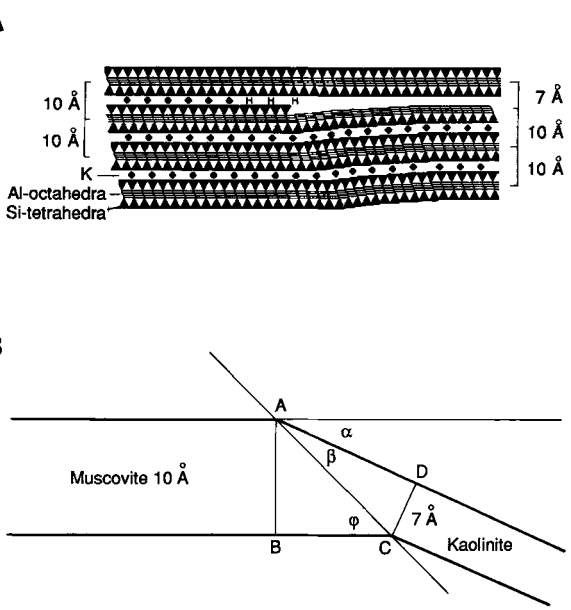

Figure 11. (A) Diagram representing the topotactic conversion of a 10-Å muscovite layer to a 7-Å kaolinite layer by replacement of K by H, followed by stripping of a Si tetrahedral sheet from one side of a 10-Å layer. (B) Geometric considerations in the topotactic alteration of muscovite to kaolinite along an oblique boundary.

one layer of kaolinite. This transformation is illustrated diagramatically in Figure 11A.

INTERPRETATIONS AND CONCLUSIONS

Weathering of the granite at Trial Hill has led to complete alteration of the plagioclase phase of the perthite to spiral halloysite tubes, whereas the potassium feldspar phase has been etched but is otherwise intact. The separate plagioclase, which originally contained muscovite patches, was altered to a very fine grained mat of platey kaolinite and some halloysite, set with patches of a coarse-grained mixture of kaolinite-muscovite.

These materials showed the alteration of muscovite to kaolinite and kaolinite to spiral halloysite and demonstrated the mechanism of formation of halloysite spirals and tubes. The variability of electron microprobe analyses indicated that compositional variation in the product minerals was finer than the diameter of the area of X-ray emission (5 μm).

Beam damage and electron probe analysis

Some electron microscope studies of mineral alteration have shown that the interface between primary and secondary minerals is susceptible to beam damage. Veblen and Buseck (1980) reported that, in complex biopyriboles, the region at the end of "zippers" tends to damage more quickly than the rest of the sample. In their study of the alteration of biotite to chlorite, Eggleton and Banfield (1985) noted rapid electron beam damage at edge dislocations in biotite and at narrow chlorite lamellae in host biotite. Spinnler (1985), quoted by Wicks and O'Hanley (1988), found that antigorite was more susceptible to beam damage at the points of inversion of the tetrahedral sheet.

The rapidly damaging mica of the present study suggests an early phase of alteration, not shown by the image or diffraction pattern, which made the mica susceptible to the electron beam. This mica was probably K-deficient, with H_3O^+ substituted for the lost K^+, based on the following: (1) AEM analyses of the electron-beam-susceptible muscovite in this study always indicated K-deficiency relative to stable, unaltered muscovite. (2) Banfield and Eggleton (1988) and Wang (1988) concluded from detailed electron microscopy of biotite weathering that the first step in that alteration is the loss of K from alternate biotite interlayers. (3) Dioctahedral phyllosilicates are apparently decreasingly stable in an electron beam in the order muscovite > montmorillonite > kaolinite > halloysite (upublished work in this laboratory). This sequence is one of increasing (OH) or H_2O, suggesting that the replacement of K^+ by H_3O^+ may have rendered the mica less stable.

Transformation of muscovite to kaolinite

As suggested above, the first stage in the alteration of muscovite was the partial substitution of K^+ by H_3O^+. If dissolution produced voids, some muscovite then appears to have transformed to smectite, as indicated by the observed increase in the interlayer spacing from 10 to 14 Å in the voids between kaolinite and halloysite.

In the absence of void space, the TEM images of the contact between muscovite and kaolinite indicate that the transformation was topotactic, with each 10-Å muscovite layer being transformed to a 7-Å kaolinite layer. Generally, the contact between the two phases was parallel, or very nearly so. Some contacts were inclined at a very acute angle to the layering, and here the layers in the kaolinite were no longer parallel to the layers in the muscovite. Such a low-angle boundary might be expected to have resulted from the volume loss and consequent collapse, if a 10-Å structure converted to a 7-Å structure.

The geometric conditions for transformation of one layer of muscovite to one layer of kaolinite were tested against alternate hypotheses. With reference to Figure 11B, if the contact between the two phases is inclined at angle ψ to the layering in the muscovite, then the two triangles ABC and ADC have a common hypotenuse, AC. The angle between the muscovite layers and the discontinuity, ψ, and the angle between the kaolinite and the discontinuity, β, must have the relationship: $\sin\beta = (7 \sin\psi)/10$. From this relationship, the angle β may be calculated for a transformation of a single

10-Å layer of muscovite to a single 7-Å layer of kaolinite, where angle ψ is 6.3° (measured from the photomicrograph). From the above relationship, angle β should be 4.4°. The actual value of β, measured from the same photomicrograph, is 4.8°, a very close agreement.

To test alternate hypotheses, similar calculations were made on the basis of a transformation of one layer of muscovite to two layers of kaolinite and two layers of muscovite to one layer of kaolinite. Theoretical values for β of 8.9° and 2.2° were obtained, respectively, which are significantly different from the actual value of 4.8°. Thus, the hypothesis of transformation of one layer of muscovite to one layer of kaolinite is supported by geometric considerations.

Transformation of kaolinite to halloysite

SEM and, particularly, TEM evidence from several mixed kaolinite and halloysite materials, all derived from weathering of different feldspars at Trial Hill, indicates that platey kaolinite converted to spiral halloysite rods. The process appears to have been initiated by a loss of structural rigidity at points along the kaolinite crystal, interpreted as hydration to halloysite. At these points the mixed grain began to curl. During the early parts of this process remnants of kaolinite, indicated by mottled diffraction contrast within the halloysite, provided a localized rigidity, which restricted curvature and caused the halloysite to curl into rods having a spiral, polygonal cross section. Because the relict kaolinite was also progressively altered, this rigidity was lost and the rods converted to those with circular or oval cross sections. Dissolution and reprecipitation of halloysite at a later stage may have resulted in separate halloysite rods having an annular cross section.

The full paragenesis of the alteration of kaolinite to halloysite is best illustrated by the clay pseudomorphs after plagioclase and the intergrown kaolinite and birefringent muscovite from Trial Hill. Although no kaolinite plates were found in the clay pseudomorphs after perthitic plagioclase, linear parts of polygonal halloysite spirals, which showed mottled diffraction contrast, strongly suggest that kaolinite was a precursor. Perthitic clays, however, showed a spectacular variety of halloysite cross sections.

Tazaki (1981) noted a correlation between tubular halloysite morphology and a low iron content, high-iron halloysites tending to spherical structures. The low iron content of the halloysite of Trial Hill and the kaolinite from which it was derived, match well with Tazaki's low-iron, tubular halloysite.

If muscovite alters to kaolinite, the collapse of the muscovite structure should produce a volume decrease of about 30%. This process could have given rise to the observed lenticular voids and partings, leaving space for the kaolinite to become fanned, and allowing access of fluids for hydration of kaolinite to halloysite. Sufficient space would then have been available for halloysite to curl into spiral tubes. Conversely, where voids are lacking, there would be less fluid access, and, even if hydration had taken place, halloysite tubes would not have formed, due to a lack of freedom to curl. Where the plagioclase of a perthite has been altered, only halloysite rods and no platey kaolin occur. The relatively rigid structure of the relict potassium feldspar may have locally resisted collapse of the surrounding saprolite and provided abundant open space for ingress of water and freedom for halloysite spiral development.

ACKNOWLEDGMENTS

The authors acknowledge assistance by the staff of the Australian National University and CSIRO, especially Qiming Wang for additional TEM and AEM which demonstrated Al loss in the analytical process. N. Ware of the Research School of Earth Sciences (microprobe), J. S. Preston and R. Heady of the Forestry Department (SEM), P. J. Barlow of the Research School of Chemistry (TEM), J. FitzGerald of the Research School of Earth Sciences (AEM) and C. Foudoulis of the Geology Department (XRD, ion beam milling and photography) provided essential support. L. Widmeier (ANU) and C. R. Steel (CSIRO) annotated the photographs and C. R. Steel drafted the figures. D. Nahon and K. Tazaki are thanked for critical reviews of the manuscript. Particular thanks are due to Renison Goldfields Consolidated Ltd., for logistical field support and to Eddie Harper (tin miner and poet) for his assistance and hospitality. Australian Research Grant Scheme Grant No. E8115611R enabled the research to be carried out and is acknowledged with appreciation.

REFERENCES

Bailey, S. W. (1989) Halloysite: A critical assessment: in abstracts, *9th International Clay Program and Abstracts, Int. Clay Conf., Strasbourg, 1989.*

Banfield, J. F. (1985) The mineralogy and geochemistry of granite weathering: M.Sc. thesis, Australian National Univ., Canberra, Australia, 130 pp.

Banfield, J. R. and Eggleton, R. A. (1988) Transmission electron microscope study of biotite weathering: *Clays & Clay Minerals* **36,** 47–60.

Eggleton, R. A. and Banfield, J. F. (1985) The alteration of igneous biotite to chlorite: *American Mineral.* **70,** 902–910.

Hanson, R. F., Zamora, R., and Keller, W. D. (1981) Nacrite, dickite and kaolinite in one deposit at Nayarit, Mexico: *Clays & Clay Minerals* **29,** 451–453.

Keller, W. D. (1982) Kaolin—A most diverse rock in genesis, texture, physical properties and uses: *Geol. Soc. Amer. Bull.* **93,** 27–36.

Keller, W. D. and Hanson, R. F. (1975) Dissimilar fabrics by scan electron microscopy of sedimentary versus hydrothermal kaolins in Mexico: *Clays & Clay Minerals* **23,** 201–204.

Robertson, I. D. M. (1990) Weathering at the Trial Hill Tin Mine—Queensland: *Centre for Australian Regolith Studies, Occ. Publ.* **No. 1,** 47 pp.

Spinnler, G. E. (1985) HRTEM study of antigorite, pyroxene-serpentine reactions and chlorite: Ph.D. thesis, Arizona State Univ., Tempe, Arizona, 268 pp.

Tazaki, K. (1981) Analytical electron microscopic studies of halloysite formation processes—Morphology and composition of halloysite: in *Proc. Int. Clay Conf., Bologna and Pavia, 1981,* H. van Olphen and F. Veniale, eds., Elsevier, Amsterdam, 573–584.

Tazaki, K. and Fyfe, W. S. (1987) Primitive clay precursors formed on feldspar: *Can. J. Earth Sci.* **24,** 506–527.

Veblen, D. R. and Buseck, P. R. (1980) Microstructures and reaction mechanisms in biopyriboles: *Amer. Mineral.* **65,** 599–623.

Wang, Qiming (1988) Mineralogical aspects of monzonite alteration: An investigation by electron microscopy and chemistry: Ph.D. thesis, Australian National University, Canberra, Australia, 192 pp.

Wicks, F. J. and O'Hanley, D. S. (1988) Serpentine minerals: Structure and petrology: in *Hydrous Phyllosilicates (Exclusive of Micas),* S. W. Bailey, ed., *Reviews in Mineralogy* **19,** Mineralogical Society of America, Washington, D.C., 91–167.

(Received 6 May 1989; accepted 3 October 1990; Ms. 1911)